Adsorption properties of chalcogen atoms on a golden buckyball Au_{16}^- from first principles

2011 J. Phys.: Condens. Matter 23 505301

(http://iopscience.iop.org/0953-8984/23/50/505301)

J. Phys.: Condens. Matter **23** (2011) 505301 (7pp) doi:10.1088/0953-8984/23/50/505301

Adsorption properties of chalcogen atoms on a golden buckyball Au_{16}^- from first principles

Seoung-Hun Kang, Gunn Kim[1] and Young-Kyun Kwon

Department of Physics and Research Institute for Basic Sciences, Kyung Hee University, Seoul 130-701, Korea

E-mail: gunnkim@khu.ac.kr and ykkwon@khu.ac.kr

Received 1 September 2011, in final form 9 November 2011
Published 30 November 2011
Online at stacks.iop.org/JPhysCM/23/505301

Abstract

Using first-principles density functional theory, we investigate the adsorption properties of chalcogen elements (oxygen and sulfur) on an anionic golden nanocage Au_{16}^- and its effects on the structural and electronic properties of the golden cage. In particular, we find that when a sulfur atom is encapsulated inside Au_{16}^-, its bonding character with Au atoms appears ionic due to electron transfer from sulfur to the gold nanocage. In contrast, the exohedrally adsorbed S atom tends to have strong orbital hybridization with the golden nanocage. For an oxygen adsorption case, electrons from the golden cage tend to be shared with the adsorbed O atom exhibiting strong orbital hybridization, regardless of its adsorption sites. To investigate the transition behaviors between the most stable exohedral and endohedral adsorption configurations, we calculate the activation and reaction energies in the transition. The oxygen atom experiences a lower energy barrier than the sulfur atom due to its smaller atomic radius. Finally, we explore the vibrational properties of S- or O-adsorbed Au_{16}^- buckyballs by calculating their infrared spectra.

(Some figures may appear in colour only in the online journal)

1. Introduction

Since their first discovery, gold nanoparticles, which are about 10–100 nm in diameter, have been explored by many researchers. They are expected to act as new catalysts, since they are much more reactive than their bulk counterparts which cannot act as catalysts due to their relative inertness. Moreover, gold nanoparticles can be utilized by functionalizing their surfaces. For gold bulk surfaces, it is well known that organic molecules with the thiol (–SH) group can easily anchor to the surfaces through favorable S–Au bonding and form a self-assembled monolayer (SAM). Due to the special S–Au interaction, different chemicals with the thiol group can functionalize Au surfaces for various purposes [1–5], especially for diverse biomedical applications [6].

More recently, even smaller gold clusters have been discovered and studied experimentally and theoretically. It is found that small clusters, either neutral or anionic, with a dozen Au atoms form planar structures [7–9], while those with more Au atoms tend to form three-dimensional (3D) configurations. Twelve Au atoms is the critical size for the two-dimensional (2D) to 3D structural transition [10, 11]. The global minimum structure of Au_{12}^- is 3D with a nearly degenerate 2D isomer coexisting in the cluster beam [12]. Among small gold clusters, the most intriguing structures are the golden cages Au_n^- ($16 \leq n \leq 18$) with empty interiors [13, 14]. In particular, Au_{16}^- has the highest symmetry (T_h) with an inner diameter of ≈5.5 Å [13], suggesting a possibility of endohedral doping in analogy to the endohedrally doped carbon fullerenes. Numerous theoretical and experimental

[1] Present address: Department of Physics, Sejong University, Seoul 143-747, Korea

studies of golden cages doped with metal atoms have been reported [12, 15–23].

Fullerene molecules such as C_{60}, C_{70}, C_{80}, etc and their derivatives have drawn attention due to their appealing electronic, optical, and electrochemical properties [24–28]. They have been used for various purposes such as chemical and biological applications. In analogy with fullerene derivatives, we consider golden cage derivatives. As discussed above, a sulfur atom can act as a linker between an organic molecule and an inorganic golden buckyball, which may play a role as a quantum dot applied to future electronic and optical devices.

Here, we report our study on the golden cage anion, Au_{16}^-, doped with a S or an O atom, rather than molecules containing a S or an O atom[2]. As mentioned above, the golden cage could be easily functionalized with a S atom. Similarly, an O atom can be considered since it has the same valence electrons as sulfur. Moreover, oxidation is an important issue for gold nanostructures due to their relatively high reactivity in comparison with their bulk counterpart. Therefore, it is of great importance to understand the adsorption properties of the chalcogen elements on the golden nanocage. We also investigated their vibrational properties by calculating infrared (IR) active vibrational modes, and the activation energy barriers in the transition between the most stable exohedral and endohedral doping configurations as well as their reaction energies.

2. Computational details

To explore the adsorption properties of sulfur and oxygen atoms on Au_{16}^-, we carried out first-principles calculations within density functional theory (DFT) implemented in the DMol^3 package [30]. We used the spin polarized generalized gradient approximation (GGA) with the Perdew–Burke–Ernzerhof (PBE) functional [31] to describe the exchange–correlation (XC) functional. A double numerical polarized basis set was chosen with a real-space cutoff of 6.5 Å to expand the electronic wave functions. The scalar relativistic effects were included in the all-electron calculation. The octupole scheme for the multipolar fitting procedure and a fine grid scheme for the numerical integration were employed for an accurate evaluation of the charge density. To obtain the equilibrium structures of the charged golden cage and its various S- or O-adsorbed derivatives, we performed structure relaxations using the Broyden–Fletcher–Goldfarb–Shanno algorithm [32–37] without any symmetry constraints until all the atomic forces became smaller than 4×10^{-4} Ha Å^{-1}. The electronic structure calculations were also repeated using a plane-wave basis set with an energy cutoff of 500 eV. The ionic potentials were described by projector-augmented waves [38] implemented in the Vienna *ab initio* simulation package (VASP) [39]. We used the PBE functional [31] for the XC functional as in the DMol^3 calculations. The general features of the calculational results from the two packages (DMol^3 and VASP) were almost identical.

To search for a three-dimensional trajectory for the reaction path between reactants and products during the atomic encapsulation, the linear synchronous transit and quadratic synchronous transit (LST/QST) calculations [40, 41] were carried out with conjugate gradient minimization [42]. Since the transition state obtained by the LST/QST may not be the transition state connecting the intended reactant and product for a particular reaction step, we calculated the minimum energy path and the activation energy barrier using the nudged elastic band (NEB) method [43].

We also evaluated vibrational spectra for our model systems, especially focused on IR active modes. After obtaining optimized geometries, the vibrational spectra were calculated by diagonalizing the force constant matrix [44, 45]. The intensities of the IR active modes were determined from the derivative of the electric dipole moment.

3. Results and discussion

Our structural optimization shows that an anionic Au_{16}^- cluster forms a truncated tetrahedron with tetrahedral symmetry T_d. Based on geometrical symmetry, we considered nine different sites where an adsorbate can be bound, as shown in figure 1. In a truncated tetrahedron, there are four truncated triangular facets, defined as TR1, shown in figure 1(a), and four hexagonal facets. In particular, each hexagonal facet in the Au_{16}^- cluster is divided into six triangles, which are geometrically different from TR1 and are classified into two types, TR2 and TR3. As shown in figures 1(b) and (c), TR2 shares an edge with a neighboring TR1 and two edges with two TR3 triangles in the same hexagonal facet, while TR3 has a common junction with another TR3 located on a neighboring hexagonal facet, and two junctions with two TR2 triangles in the same hexagonal facet. Three TR2 and three TR3 triangles are arranged alternately on each hexagonal facet. Edges shared by two neighboring triangles or bridges between two Au atoms can be classified into three types of edges or bridges, BR1, BR2, and BR3, as displayed in figures 1(d)–(f). BR1 is shared by TR1 and TR2; BR2 by TR2 and TR3 in the same hexagonal facet; and BR3 by two TR3 triangles, one in a hexagonal facet and the other in a neighboring hexagonal facet. In addition, there are two types of vertices or atop sites, AT1 and AT2. AT1 represents twelve equivalent vertices forming four TR1 triangles, and the remaining four vertices located at the center of each hexagonal facet are of the other type, AT2. Overall, there exist eight different adsorption sites on the outer surface of the Au_{16}^- cage, and one more site at the center (CTR) of the golden cage, which was also considered as an 'adsorption' site for endohedral doping of a S or an O atom.

For each configuration shown in figure 1, we performed geometrical relaxation to obtain the equilibrium structure of XAu_{16}^-, where X is either a S or an O atom, and calculated the binding energy E_b defined by

[2] Atomic S or O can be produced by various chemical reactions, for example an oxygen atom is a product of $CO + O_2 \rightarrow CO_2 + O$ (see [29]).

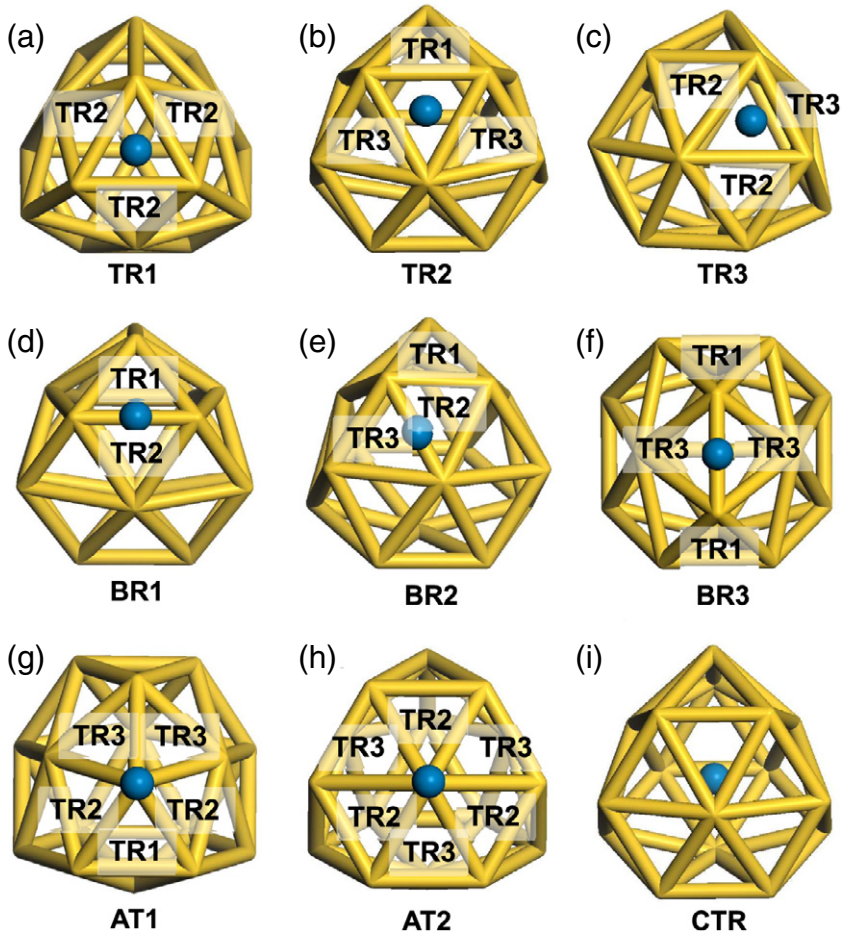

Figure 1. Atomic model structures of the sulfur or oxygen atom adsorbed on the golden buckyball (Au_{16}^-). There are nine adsorption sites of the adsorbate: (a)–(c) three inequivalent triangular sites, TR1, TR2, and TR3; (d)–(f) three different bridge sites, BR1, BR2, and BR3; (g), (h) two dissimilar atop sites, AT1, AT2; and (i) the central site, CTR, for encapsulation. See the text for the detailed classification of the nine adsorption sites.

$$E_b = E[Au_{16}^-] + E[X] - E[XAu_{16}^-],$$

where $E[XAu_{16}^-]$ and $E[Au_{16}^-]$ are the total energies of the golden cage with and without X, respectively, and $E[X]$ stands for the energy of an isolated X atom. Note that the positive (negative) value of E_b indicates that the adsorption process is exothermic (endothermic). The binding energy of the sulfur atom on the outer surface of Au_{16}^- varies site by site. We find that triangular sites (TR1, TR2, and TR3) are preferred by the sulfur atom as in the thiol-adsorbed Au(111) surface. The TR2 configuration is the most stable adsorption site with the greatest binding energy of 3.93 eV, and the TR1 (TR3) configuration has a binding energy of 3.86 eV (3.78 eV). Its binding energy on the bridge sites (BR1, BR2 and BR3) ranges from 3.48 to 3.61 eV; these values are a little smaller than on triangular sites. Atop sites (AT1 and AT2) are even less preferable (∼2.13 eV on AT2) than the triangular sites. It was found that the S atom initially placed at AT1 spontaneously moved to TR2 during the structural relaxation implying that AT1 is an unstable adsorption site. We also calculated its encapsulation energy, which is defined by the energy gain due to the endohedral doping, or the binding energy at CTR. In contrast to the well-known results that some metal adatoms (such as Li, Na and Cu) tend to be encapsulated into the Au_{16}^- cage [17, 20], rather than adsorbed on the outer surface, our calculated encapsulation energy (0.37 eV) of the sulfur atom is much smaller than the binding energies on the outer surface. All calculated energy values are summarized in table 1.

For an oxygen atom, on the other hand, its encapsulation energy of 0.91 eV is a little larger than that for a sulfur atom. Similarly to the sulfur adsorption, all the outer adsorption sites are preferred to endohedral doping. The AT1 site was found to be unstable for the O atom as well. The oxygen atom binds to the triangular sites with the binding energy ranging from $E_b \approx 3.19$ to 3.43 eV, and to the bridge sites from $E_b \approx 3.24$ to 3.48 eV, whereas $E_b \approx 2.20$ eV on the AT2 atop site. The overall trend in the binding energy of the oxygen atom is quite similar to that of the sulfur atom. A small, but important difference is that the most stable adsorption site for the oxygen atom is a bridge site (BR3), while that of the sulfur atom is a hollow site (TR2). This difference is attributed to the different orbital characters of O 2p and S 3p. The distances between the adsorbate and its nearest gold atom (d_{Au-X}, where X = S or O) are listed in table 1.

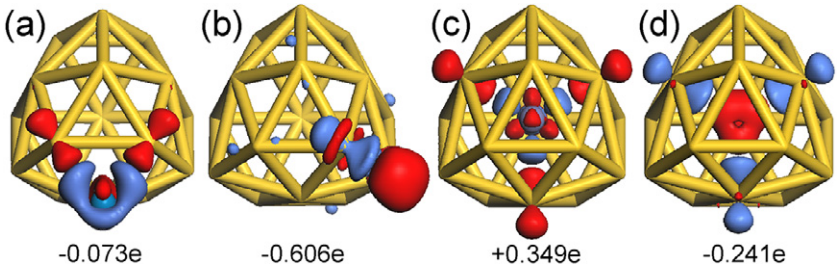

Figure 2. The charge density differences for the most stable exohedral adsorption structures of SAu_{16}^- (a) and OAu_{16}^- (b), and for the endohedral doping of S (c) and O (d) in Au_{16}^-. S and O atoms are located at TR2 in (a) and BR3 in (b), respectively. The electron accumulation is represented by dark color (red), while the depletion is in light color (blue). The isovalue is $\pm 0.005\ e\ \text{Å}^{-3}$. The value given at the bottom of each structure is the amount of electronic charge transferred according to the Mulliken population analysis.

Table 1. The binding energy, E_b, the binding distance between the adsorbed atom and its nearest gold atom in the golden buckyball, d_{Au-X} (X = S, O), and the amount of electronic charge transferred from Au_{16}^- to the dopant atom, S or O, ΔQ, at the different adsorption sites shown in figure 1. The data for the AT1 site were omitted since it is unstable for both S and O adsorption.

	S on Au_{16}^-			O on Au_{16}^-		
Site	E_b (eV)	d_{Au-S} (Å)	ΔQ (e)	E_b (eV)	d_{Au-O} (Å)	ΔQ (e)
TR1	3.86	2.40	−0.106	3.43	2.11	−0.620
TR2	3.93	2.35	−0.073	3.24	2.18	−0.591
TR3	3.78	2.36	−0.070	3.19	2.10	−0.603
BR1	3.61	2.29	−0.123	3.36	2.01	−0.583
BR2	3.48	2.31	−0.104	3.24	2.00	−0.583
BR3	3.58	2.27	−0.133	3.48	1.99	−0.606
AT2	2.13	2.20	−0.219	2.20	1.87	−0.514
CTR	0.37	2.49	+0.349	0.91	2.32	−0.241

For comparison, we also calculated the adsorption energy of S and O atoms on Au(111) and Au(211) surfaces. We found that the Au(211) surface is more reactive than the Au(111) surface for the adsorption of S and O atoms, since their binding energies on the Au(211) surface are larger by about 0.1–0.5 eV than those on the Au(111) surface and similar to those on the Au_{16}^- cage.

To examine the charge redistribution induced by S or O atom adsorption, we calculated the charge density difference, as displayed in figure 2. The charge transfer ΔQ between the adsorbate and the golden cage was also calculated using the Mulliken population analysis. The sulfur (oxygen) atom accepts electrons of ∼0.07 e (∼0.61 e) for the most stable exohedral doping structure. Interestingly, the endohedrally doped sulfur atom donates ∼0.35 e to the golden cage, whereas the oxygen counterpart accepts ∼0.24 e from the Au_{16}^- cage. This implies that the confined space inside the golden cage determines the actual size of the dopant. Since the neutral S atom is larger than the neutral O atom, the former reduces its size to fit into the cage by yielding its electrons to Au_{16}^- to be a positive ion. Such an opposite charge transfer may be a reason for the smaller encapsulation energy of the S atom than that of the O atom. Moreover, it was found that the inner space of the golden cage became expanded due to the encapsulated sulfur atom.

Figure 3(a) displays the highest occupied molecular orbitals (HOMO) and lowest unoccupied molecular orbitals (LUMO) of the most stable exohedrally adsorbed cage structures of SAu_{16}^- and OAu_{16}^- and their encapsulated structures. The HOMO and LUMO of the pristine Au_{16}^- are also given for comparison. As shown in the figure, S 3p and O 2p orbitals form antibonding characters with Au 5d orbitals. We calculated the projected densities of states to further analyze the bonding characters between the adsorbate and the golden cage. Only $S@Au_{16}^-$ exhibits an ionic bonding character, whereas $O@Au_{16}^-$ as well as the exohedrally doped structures shows strong orbital hybridization. Figure 3(b) shows the energy levels near the Fermi level of each structure shown in figure 3(a). The existence of the adsorbate appears to modify the electronic structures quite strongly. The energy gap between HOMO and LUMO decreases from that of the pristine Au_{16}^-, whose HOMO–LUMO energy gap is about 1.37 eV. The HOMO–LUMO energy gap is 0.98 eV (0.42 eV) for the most stable SAu_{16}^- (OAu_{16}^-), and 1.07 eV (0.53 eV) for the endohedral structure of $S@Au_{16}^-$ ($O@Au_{16}^-$). This implies that various golden cage derivatives would be stable themselves and could be utilized for different optoelectronic devices. Moreover, $S@Au_{16}^-$ may be chemically less reactive than the other doped golden cages due to its relatively larger HOMO–LUMO gap.

Figure 4 shows a schematic diagram of the energy profile exhibiting an activation barrier (E_a) in the transformation between the stable exohedral and endohedral adsorption configurations, as well as their reaction energies (E_r) defined by the energy difference between the reactant and the product. Table 2 summarizes the activation barriers (E_a) and the reaction energies (E_r) of our model structures. We considered three paths (TR1 → CTR, TR2 → CTR and TR3 → CTR)

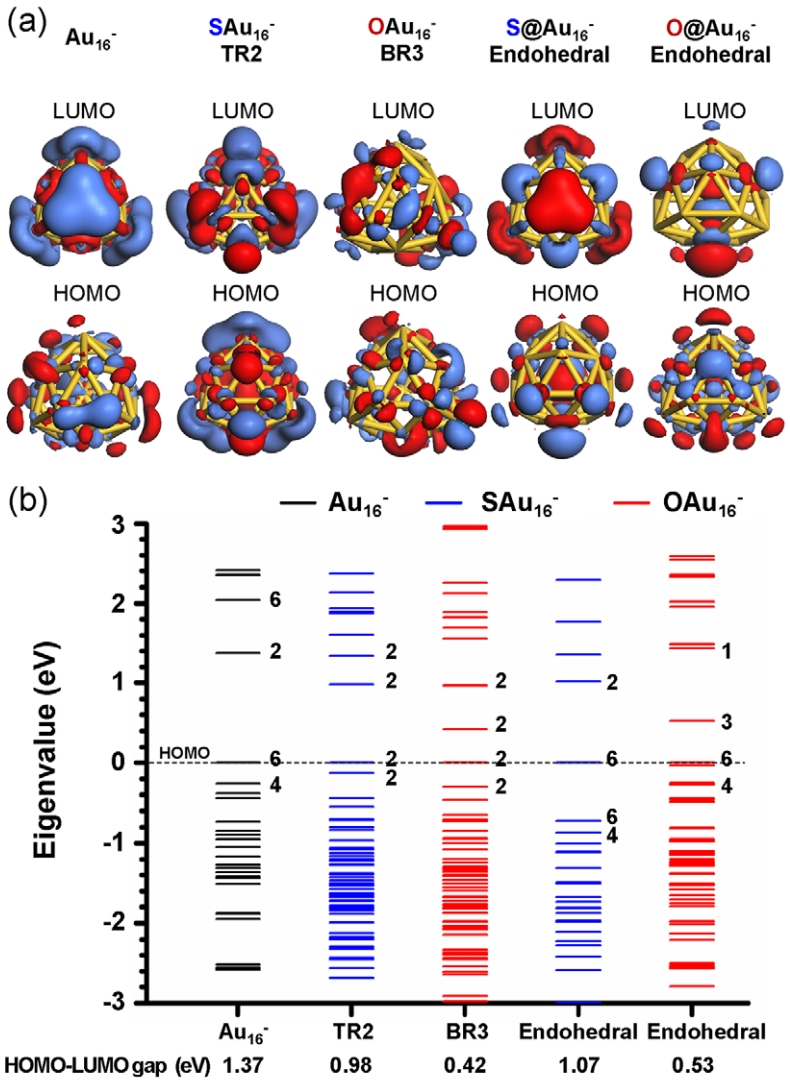

Figure 3. (a) Highest occupied molecular orbitals (HOMO) and lowest unoccupied molecular orbitals (LUMO) of the pristine Au_{16}^- cage, the most stable exohedral adsorption structures of SAu_{16}^- and OAu_{16}^-, and the endohedrally doped structure of $S@Au_{16}^-$ and $O@Au_{16}^-$. The isovalue is $\pm 0.02\ e\ \text{Å}^{-3}$. (b) Energy levels near the HOMO and LUMO for the five structures in (a). The numbers written right next to the energy levels represent the degeneracies of each level. The HOMO level is set to zero. The HOMO–LUMO energy gap is given for each structure in eV.

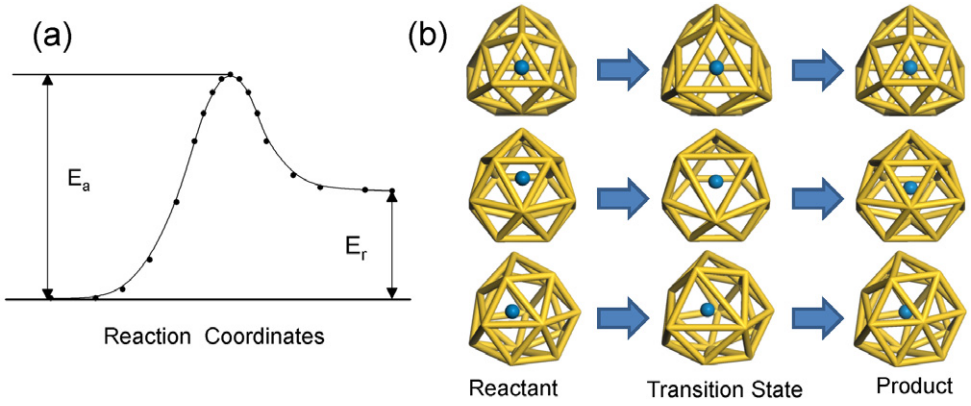

Figure 4. (a) Schematic energy profile along the reaction coordinates. The dots represent the energies of the replicas in the transformation in the NEB method. (b) Model configurations in the reaction path from the reactants, the three stable exohedral configurations (TR1, TR2 and TR3) of the S and O atoms on Au_{16}^-, to the products, the endohedral structures (CTR), with the transition states.

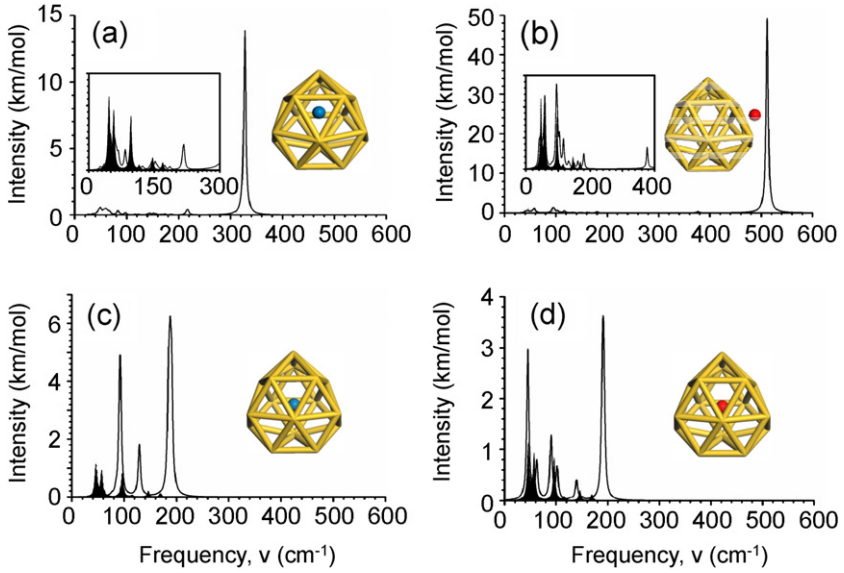

Figure 5. The IR active modes for the most stable exohedral adsorption structures of (a) SAu_{16}^- (TR2) and (b) OAu_{16}^- (BR3), and for endohedral doping of (c) $S@Au_{16}^-$ and (d) $O@Au_{16}^-$. The IR active modes for the pristine Au_{16}^- are displayed in dark color. Detailed IR spectra at frequencies below (a) $\nu = 300$ and (b) $\nu = 400$ cm^{-1} are shown as insets for the most stable exohedral cases. The IR modes for the pristine Au_{16}^- are represented in solid black.

since any triangular site can be a gate for dopant insertion. The activation barriers of the O atom along the three paths are lower than those of the S atom by 0.64 eV (TR1 → CTR), 1.10 eV (TR2 → CTR) and 0.82 eV (TR3 → CTR). This is attributed to the smaller atomic radius of oxygen than that of sulfur. We also found the same trend in the reaction energies. During encapsulation of the dopant atom, the Au–Au distances, d_{Au-Au}, are maximally stretched in the transition state. As listed in table 2, the edges of a triangle in Au_{16}^- were more elongated for the encapsulation of the S atom than for the O atom. Note that such encapsulation events would not occur at temperatures lower than the melting temperature of the golden cage since the activation barriers are very high compared to temperatures lower than the melting temperature of the golden cage. We estimated the probability for this event to occur to be at most 10^{-11} s^{-1}. However, such events could occur with the help of light or e-beam irradiation. For example, cis–trans conformation change of the azobenzene molecule was made by light-driven or electron-induced isomerization [46] and e-beam irradiation fused C_{60} molecules inside carbon nanotubes [47].

We calculated the IR spectra of the most stable exohedral adsorption configurations, SAu_{16}^- and OAu_{16}^-, and the endohedral configurations, $S@Au_{16}^-$ and $O@Au_{16}^-$. Figure 5 shows our IR results for these selected structures. We expect that different IR spectra can be used to distinguish between exohedrally and endohedrally doped isomers and also between SAu_{16}^- and OAu_{16}^-. For comparison, we also calculated the IR spectrum for the pristine Au_{16}^- cage and found that its dominant IR intensities were observed in the frequency range below $\nu \approx 200$ cm^{-1}, since Au is a heavy element and thus $\nu \propto 1/\sqrt{m}$, where m is atomic mass. In particular, three modes with strong intensities were observed at $\nu \approx 45$, 56, and 96 cm^{-1} corresponding to an Au–Au bond stretching mode and several weak modes, respectively. Interestingly, the S atom insertion suppresses the first two modes peaked near $\nu \approx 45$–50 cm^{-1} existing in the pristine cage, as seen in figure 5(c), but the O atom insertion keeps them active as displayed in figure 5(d). Regardless of the dopant type the encapsulation gives rise to the strong IR peak at $\nu \approx 200$ cm^{-1}. In the cases of exohedrally doped golden cages, we found very large IR peaks at $\nu \approx 327$ and 511 cm^{-1} corresponding to Au–S and Au–O vibrational modes, respectively, as shown in figures 5(a) and (b). If the force constants may be assumed to be identical for OAu_{16}^- and SAu_{16}^-, it is clear that the vibrational frequencies are inversely proportional to $\sqrt{m}$, that is,

$$\sqrt{\frac{m_S}{m_O}} \approx \sqrt{\frac{32}{16}} \approx \frac{511}{327} = \frac{\nu_{OAu_{16}^-}}{\nu_{SAu_{16}^-}},$$

where $m_S \approx 32$ and $m_O \approx 16$ in atomic weight. Such high frequency modes do not occur in endohedrally doped golden

Table 2. The activation energy barriers E_a for the transition from three triangular sites (TR1, TR2 and TR3) to the center (CTR) of the golden cage as well as their reaction energies E_r, and the maximally elongated distance Δd_{Au-Au} from the equilibrium distance between two neighboring Au atoms in each triangle during the transition process of encapsulation. All energy and distance values are given in eV and Å, respectively.

System		E_a	E_r	Δd_{Au-Au} (Å)
SAu_{16}^-	TR1 → CTR	4.28	3.49	+1.03
	TR2 → CTR	3.98	3.56	+0.99, +0.84
	TR3 → CTR	3.68	3.41	+0.81, +0.74
OAu_{16}^-	TR1 → CTR	3.64	2.52	+0.65
	TR2 → CTR	2.88	2.33	+0.66, +0.46
	TR3 → CTR	2.86	2.28	+0.64, +0.42

cages because the potential energy inside the cage is nearly flat for a small displacement near the center (i.e., small force constant). The general trend is that exohedral doping yields larger intensities than endohedral doping at higher frequencies.

4. Conclusion

In summary, we investigated the adsorption effects of sulfur and oxygen atoms on the structural and electronic properties of a golden cage Au_{16}^- using scalar relativistic all-electron density functional calculations. When the S atom is encapsulated in Au_{16}^-, the adsorption character appears ionic. In particular, electrons are donated to Au_{16}^- from the encapsulated sulfur atom. For exohedral doping, in contrast, we observed strong orbital hybridization between the dopant atom and the Au atoms. We also calculated the activation energy barriers of the transition between the stable exohedral and endohedral adsorption configurations, as well as their reaction energies. Our results show that the activation barrier in OAu_{16}^- is lower than in SAu_{16}^- by ∼1 eV. This is associated with the smaller atomic radius of oxygen than that of sulfur. For the calculations of the IR spectra, we found that exohedral doping provokes larger intensities than endohedral doping at higher frequencies. Our results help in understanding the adsorption properties of doped S and O atoms on the golden cage, which may be of importance for the design of new types of small gold nanocluster derivatives. Based on our present work, we will further investigate the adsorption properties of tri-atomic molecules such as O_3, SO_2, H_2O and H_2S containing sulfur or oxygen atoms on the golden buckyball to understand its catalytic behavior.

Acknowledgment

This work was supported by a grant (KHU-20100119) from Kyung Hee University in 2010.

References

[1] Liu Z, Shen Z, Zhu T, Hou S, Ying L, Shi Z and Gu Z 2000 *Langmuir* **16** 3569–73
[2] Aslam M, Mulla I S and Vijayamohanan K 2001 *Langmuir* **17** 7487–93
[3] Levicky R, Herne T M, Tarlov M J and Satija S K 1998 *J. Am. Chem. Soc.* **120** 9787–92
[4] Kim K S, Demberelnyamba D and Lee H 2004 *Langmuir* **20** 556–60
[5] Chaki N K and Vijayamohanan K 2002 *Biosens. Bioelectron.* **17** 1–12
[6] Shenoy D, Fu W, Li J, Crasto C, Jones G, DiMarzio C, Sridhar S and Amiji M 2006 *Int. J. Nanomed.* **1** 51–7
[7] Furche F, Ahlrichs R, Weis P, Jacob C, Gilb S, Bierweiler T and Kappes M 2002 *J. Chem. Phys.* **117** 6982–90
[8] Häkkinen H, Yoon B, Landman U, Li X, Zhai H J and Wang L S 2003 *J. Phys. Chem.* A **107** 6168–75
[9] Häkkinen H, Moseler M and Landman U 2002 *Phys. Rev. Lett.* **89** 033401
[10] Huang W and Wang L 2009 *Phys. Rev. Lett.* **102** 153401
[11] Johansson M P, Lechtken A, Schooss D, Kappes M M and Furche F 2008 *Phys. Rev.* A **77** 053202
[12] Huang W, Bulusu S, Pal R, Zeng X C and Wang L S 2009 *J. Chem. Phys.* **131** 234305
[13] Bulusu S, Li X, Wang L S and Zheng X C 2006 *Proc. Natl Acad. Sci. USA* **103** 8326–30
[14] Huang W, Bulusu S, Pal R, Zeng X C and Wang L S 2009 *ACS Nano* **3** 1225–30
[15] Walter M and Hakkinen H 2006 *Phys. Chem. Chem. Phys.* **8** 5407–11
[16] Sun Q, Wang Q, Chen G and Jena P 2007 *J. Chem. Phys.* **127** 214706
[17] Wang L M, Bulusu S, Zhai H J, Zeng X C and Wang L S 2007 *Angew. Chem., Int. Edn* **46** 2915–8
[18] Wang L M, Bulusu S, Huang W, Pal R, Wang L S and Zeng X C 2007 *J. Am. Chem. Soc.* **129** 15136–7
[19] Fa W and Yang A 2008 *Phys. Lett.* A **372** 6392–5
[20] Fa W and Dong J 2008 *J. Chem. Phys.* **128** 144307
[21] Sun Q, Wang Q, Jena P and Kawazoe Y 2008 *ACS Nano* **2** 341–7
[22] Wang L M, Bai J, Lechtken A, Huang W, Schooss D, Kappes M M, Zeng X C and Wang L S 2009 *Phys. Rev.* B **79** 033413
[23] Wang L M, Pal R, Huang W, Zeng X C and Wang L S 2009 *J. Chem. Phys.* **130** 051101
[24] Friedman S H, DeCamp D L, Sijbesma R P, Srdanov G, Wudl F and Kenyon G L 1993 *J. Am. Chem. Soc.* **115** 6506–9
[25] Prato M and Maggini M 1998 *Acc. Chem. Res.* **31** 519–26
[26] Echegoyen L and Echegoyen L E 1998 *Acc. Chem. Res.* **31** 593–601
[27] Guldi D M and Prato M 2000 *Acc. Chem. Res.* **33** 695–703
[28] Guldi D M and Asmus K D 1997 *J. Phys. Chem.* A **101** 1472–81
[29] Gao Y, Shao N, Pei N, Chen Z and Zeng X C 2011 *ACS Nano* **5** 7818–29
[30] Delley B 1990 *J. Chem. Phys.* **92** 508–17
[31] Perdew J P, Burke K and Ernzerhof M 1996 *Phys. Rev. Lett.* **77** 3865–8
[32] Broyden C G 1970 *J. Inst. Math. Appl.* **6** 76–90
[33] Fletcher R 1970 *Comput. J.* **13** 317–22
[34] Fletcher R 1987 *Practical Methods of Optimization* (New York: Wiley)
[35] Goldfarb D 1970 *Math. Comput.* **24** 23–6
[36] Shanno D F 1970 *Math. Comput.* **24** 647–56
[37] Shanno D F and Kettler P C 1970 *Math. Comput.* **24** 657–64
[38] Kresse G and Joubert D 1999 *Phys. Rev.* B **59** 1758–75
[39] Kresse G and Furthmüller J 1996 *Phys. Rev.* B **54** 11169–86
[40] Baker J 1986 *J. Comput. Chem.* **7** 385–95
[41] Cerjan C J and Miller W H 1981 *J. Chem. Phys.* **75** 2800–1
[42] Govind N, Petersen M, Fitzgerald G, King-Smith D and Andzelm J 2003 *Comput. Mater. Sci.* **28** 250–8
[43] Grillo M E, Andzelm J W, Govind N, Fitzgerald G and Stark K B 2004 *Lect. Note. Phys.* **642** 207–21
[44] Herzberg G 1945 Molecular spectra and molecular structure *Infrared and Raman Spectra of Polyatomic Molecules* (New York: Van Nostrand/Reinhold)
[45] Wilsun E B, Decius J C and Cross P C 1980 *Molecular Vibrations* (New York: Dover)
[46] Choi B, Kahng S, Kim S, Kim H, Kim H W, Song Y J, Ihm J and Kuk Y 2006 *Phys. Rev. Lett.* **96** 156106
[47] Bando S, Takizawa M, Hirahara K, Yudasaka M and Iijima S 2001 *Chem. Phys. Lett.* **337** 48–54